Int. J. Heat Mass Transfer. Vol. 37, No. 2, pp. 283–291, 1994
Printed in Great Britain

0017–9310/94 $6.00 + 0.00

Heat transfer enhancement in fin-tube heat exchangers by winglet type vortex generators

G. BISWAS,† N. K. MITRA and M. FIEBIG
Institut für Thermo- und Fluiddynamik, Ruhr-Universität Bochum, 4630 Bochum 1, Germany

(*Received* 10 *December* 1992 *and in final form* 3 *June* 1993)

Abstract—Numerical investigations of the flow structure and heat transfer enhancement in a channel with a built-in circular tube and a winglet type vortex generator are presented. The geometrical configuration represents an element of a gas–liquid fin-tube crossflow heat exchanger. In the absence of the winglet type vortex generator, relatively little heat transfer takes place in the downstream of the circular tube which is a recirculation region with low velocity fluid. However, in the presence of a winglet type longitudinal vortex generator in the wake region behind the cylinder, heat transfer in this region can be enhanced as high as 240%. Results show a marked increase in overall channel heat transfer. The enhancement shows great promise in reducing the size of the heat exchangers.

INTRODUCTION

IT IS WELL known that the gas-side heat transfer coefficient in gas–liquid, fin-tube crossflow heat exchangers is small compared to that of the liquid side. The purpose of the fin is to enhance the heat transfer coefficient on the gas side to a value comparable to the liquid side. The area ratio of the fins to the tubes varies depending on the application and may reach a value of 30. Heat transfer from the fin surfaces can be enhanced by generating streamwise vortices which interact with an otherwise two-dimensional boundary layer and produce a three-dimensional complex flow that mixes near wall fluid with the free stream. These streamwise vortices can be induced by placing delta-winglets on the fin surface (Fig. 1).

It has been shown experimentally by Fiebig *et al.* [1] and Tiggelbeck *et al.* [2] that the longitudinal vortices generated by surface-mounted delta-wings and winglet pairs are indeed very effective for heat transfer enhancement. Tiggelback *et al.* [2] have also shown a marvellous sequence of flow visualization describing mechanistic viewpoints for generation and gradual deformation of streamwise vortices in the flow field. Numerical studies on related topics have been reported by Fiebig *et al.* [3], Brockmeier *et al.* [4], Biswas *et al.* [5] and Biswas and Chattopadhyay [6]. In the above mentioned numerical investigations, predictions are made through the computations of complete Navier–Stokes and energy equations. However, in all these numerical studies, the interaction between the transverse vortices, generated by the tubes and the longitudinal vortices, generated by the slender bodies was not considered. Recently, Dong [7] and Valencia [8] have conducted experimental investigations in order to study the influence of winglet type of vortex generators in a channel with a built-in circular obstacle (tube). Sanchez *et al.* [9] have computed laminar flows around a circular cylinder in a rectangular channel with a pair of delta winglets on the bottom plate of the channel. Their results show that the longitudinal vortices, generated by the winglets placed in the wake, control the spread of wake zone behind the cylinder and damp the periodic vortex street. In the present work, we perform a numerical investigation on heat transfer and flow structure in an element of a fin-tube, cross-flow heat exchanger (Fig. 2) that consists of a rectangular channel with a built-in circular tube and winglet type vortex generators. Three-dimensional Navier–Stokes and energy equations are solved and predictions are made with the help of computed results.

STATEMENT OF THE PROBLEM

Figure 3 shows the computation domain which is formed by two neighbouring fins. Obstacles in the

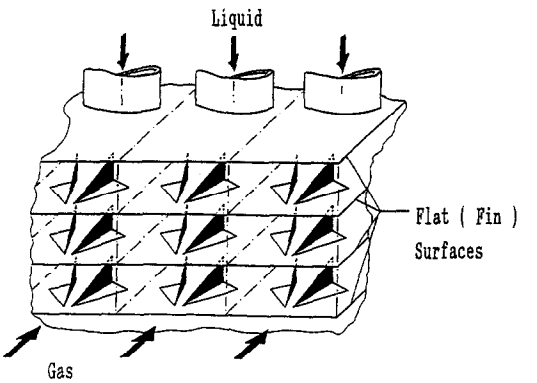

FIG. 1. Vortex generators on the flat fins.

† On leave from : Department of Mechanical Engineering, Indian Institute of Technology, Kanpur-208016, India.

NOMENCLATURE

B	channel width
b	wing span
D	tube diameter
G	$\overline{Nu}_{sa}/\overline{Nu}^{p}_{sa}$
H	channel height
h	heat transfer coefficient, $-k(\partial T/\partial y)_w/(T_w - T_b)$
k	thermal conductivity of the fluid
Nu	local Nusselt number based on bulk temperature of the fluid
$\overline{Nu}$	spanwise average Nusselt number
P	nondimensional pressure, $p/\rho U_{av}^2$
p	pressure
Pr	Prandtl number, $\mu c_p/k$
q	wall heat flux
Re	Reynolds number, $U_{av}H/\nu$
S	wing area
T	temperature
t	time
U	u/U_{av}
u	axial component of velocity
V	v/U_{av}
v	vertical component of velocity
W	w/U_{av}
w	spanwise component of velocity
X	x/H
x	axial dimension of coordinates
Y	y/H
y	vertical or normal dimension of coordinates
Z	z/H
z	spanwise dimension of coordinates.

Greek symbols

Λ	aspect ratio of the wing, b^2/S
μ	dynamic viscosity of the fluid
ν	kinematic viscosity of the fluid
τ	nondimensional time.

Subscripts

w	wall
b	bulk temperature
av	average
1	bottom fin-plate
2	top fin-plate
sa	spanwise combination of top and bottom plate.

form of a tube and a winglet are placed inside it. It has been assumed that symmetry prevails in the vertical central plane (at $z = 0$) of the heat-exchanger-element and only one-half of the heat-exchanger-element has been computed. The dimensionless equations for continuity, momentum and energy may be expressed in tensor notation as

$$\frac{\partial u_i}{\partial x_i} = 0 \tag{1}$$

$$\frac{\partial u_j}{\partial \tau} + \frac{\partial}{\partial x_j}(u_i u_j) = -\frac{\partial p}{\partial x_i} + \frac{1}{Re}\left[\frac{\partial}{\partial x_j}\left(\frac{\partial u_i}{\partial x_j} + \frac{\partial u_j}{\partial x_i}\right)\right] \tag{2}$$

$$\frac{\partial \theta}{\partial \tau} + \frac{\partial}{\partial x_j}(\theta u_j) = \frac{1}{Re\,Pr}\frac{\partial}{\partial x_j}\left(\frac{\partial \theta}{\partial x_j}\right). \tag{3}$$

In the above equations, the velocity has been nondimensionalized with the average incoming velocity U_{av} at the channel inlet; all lengths have been nondimensionalized with the channel height H; and the pressure with ρU_{av}^2. The nondimensional temperature is defined as $\theta = (T - T_r)/(T_w - T_r)$. Boundary conditions of interest in this investigation are:

Entrance (at $x = 0$):

$$u = u(y),\ v = w = 0,\ T = T_r \tag{4a}$$

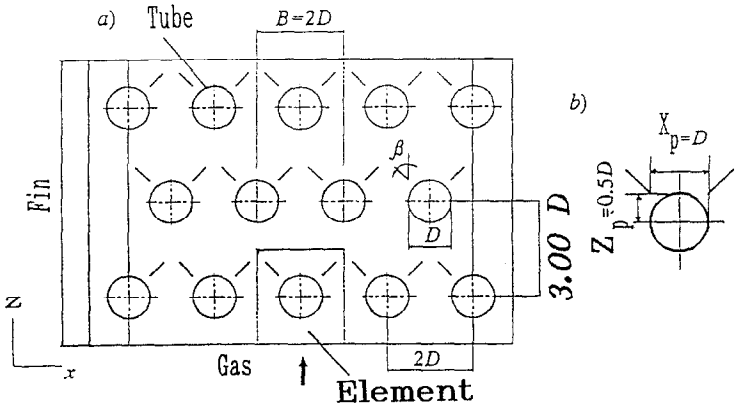

FIG. 2. An element of a heat exchanger.

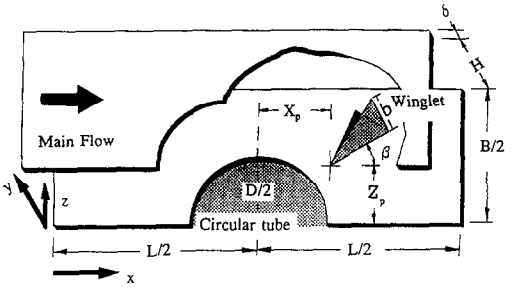

FIG. 3. Flow model for computation.

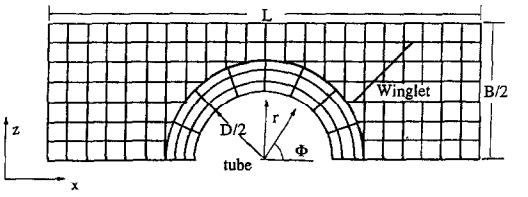

FIG. 4. Schematic plan-view of the composite grid used for computation.

Top and bottom walls (at $y = 0$ and $y = H$):

$$v = 0,\ u = w = 0,\ T = T_w \tag{4b}$$

Side wall ($z = B/2$) and midplane ($z = 0$):

$$w = (\partial v/\partial z) = (\partial u/\partial z) = (\partial T/\partial z) = 0 \tag{4c}$$

and

Exit (at $x = L$):

$$\frac{\partial^2 u}{\partial x^2} = \frac{\partial^2 v}{\partial x^2} = \frac{\partial^2 w}{\partial x^2} = \frac{\partial^2 T}{\partial x^2} = 0. \tag{4d}$$

No-slip boundary conditions for the velocities on the obstacles (the tube and the winglet) are used. The temperature of the obstacles is constant and equal to T_w. At the channel inlet, a fully developed velocity profile for the axial velocity is used.

METHOD OF SOLUTION

A modified version of Marker and Cell (MAC) method [10, 11] has been employed to solve the equations. In the numerical scheme, the computational domain of Fig. 3 is divided into a Cartesian mesh combined with a polar grid in the region of the cylinder (Fig. 4). The grid lengths in the y direction are uniform and are not shown for the sake of simplicity. Staggered grid arrangements are used in which velocity components are defined at the centre of the cell faces to which they are normal and the pressure and temperature are defined at the centre of the cell (Fig. 5). The modified MAC algorithm has the following advantages: it does not need boundary conditions for pressure, it can describe genuinely unsteady flows, it is robust and uses primitive variables which are preferable in 3-D flow calculations.

The velocity components in r, ϕ and y direction on the polar grid are interpolated out of the Cartesian values using an interpolation method of Launder and Massey [12].

Calculations are first performed only on the Cartesian grid, until a steady or a periodic solution is reached. Second order accurate boundary conditions are used to guarantee an exact description of the cylindrical obstacle (tube) on the Cartesian mesh. Close to the tube, the steepest gradients of flow properties are in the radial direction. Thus a cylindrical polar grid, in the neighbourhood of the tube, is preferred. The flow variables from Cartesian computation are then transformed on the outer ring of the polar mesh and taken as Dirichlet-boundary conditions. In the sequel, a calculation of the complete Navier–Stokes equations in the polar coordinates is performed only on the polar grid with no-slip conditions on the tube wall.

Details of the solution algorithm were discussed in

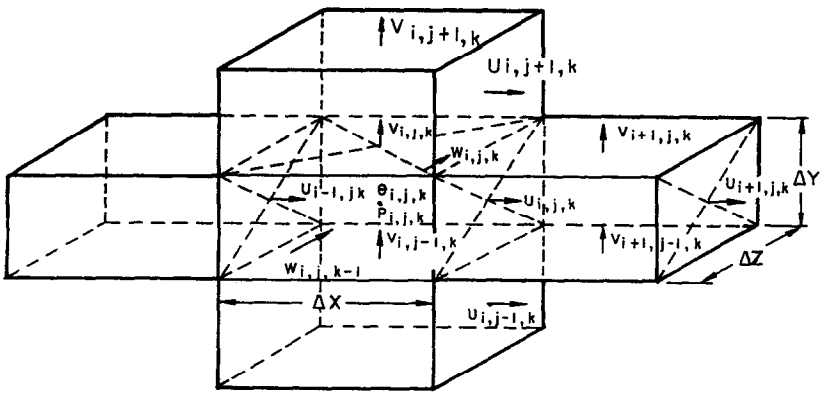

FIG. 5. Three dimensional staggered grid and location of the discretized variables.

the earlier investigations [3, 5]. A concise description is being recorded herein for a ready reference. The MAC algorithm consists of an explicit advancement in time through the momentum equations followed by an implicit, iterative pressure and velocity correction. First, a preliminary velocity field is determined explicitly for the new time from the Navier–Stokes equations making use of the pressure and other variables of the momentum equations at the previous time level. The second step serves to determine the pressure field and an updated velocity field simultaneously by an iterative procedure with the help of continuity equation until a divergence-free velocity field is reached with a prescribed upper bound; here a value of 0.0001 has been chosen. After evaluating correct velocities, the energy equations are solved with an SOR technique to determine the temperature field. The convective terms of Navier–Stokes and energy equations were discretized with a hybrid technqiue (see Raithby and Torrance [13]). The factor for the upwind contribution was restricted between 0.2 and 0.3 so that the influence of numerical viscosity is small.

For the Cartesian domain, a 14×34 cross-stream grid has been deployed. In the foregoing specification, 14 and 34 refer to the number of grids in the y and the z directions respectively. However, for a 14×34 cross-stream grid, 98 grid nodes are taken in the x direction for a nondimensional axial distance of 15. Computations have been performed on an IBM RS 6000/550 Workstation.

RESULTS AND DISCUSSION

Steady solutions are obtained up to a Reynolds number of 500. Figure 6 shows longitudinal velocity vectors on a horizontal midplane (at a distance $Y = 0.416$ from the bottom plate) of the channel. The fluid is separated behind the cylindrical obstacle and the wake region looks like a dead water zone. However, the formation of a strong recirculating vortex (transverse) bubble has not been observed. The usual point of separation for flow past circular obstacles is located approximately at a location 95° from the stagnation point. Due to the presence of the vortex generator in the wake region, a cross-stream vortical motion is generated which has a tendency to suppress the separation behind the cylinder. The downstream-shift of the point of separation and consequently formation of a narrow separated zone can be attributed to the influence of the longitudinal vortices generated by the winglet.

Figure 7(a) shows the cross-stream velocity vectors at different axial locations in the channel. Flow near the edge of the cylindrical obstacle describes the deviation from the two-dimensional crossflow structure. Driven by the spanwise pressure gradient, a horseshoe

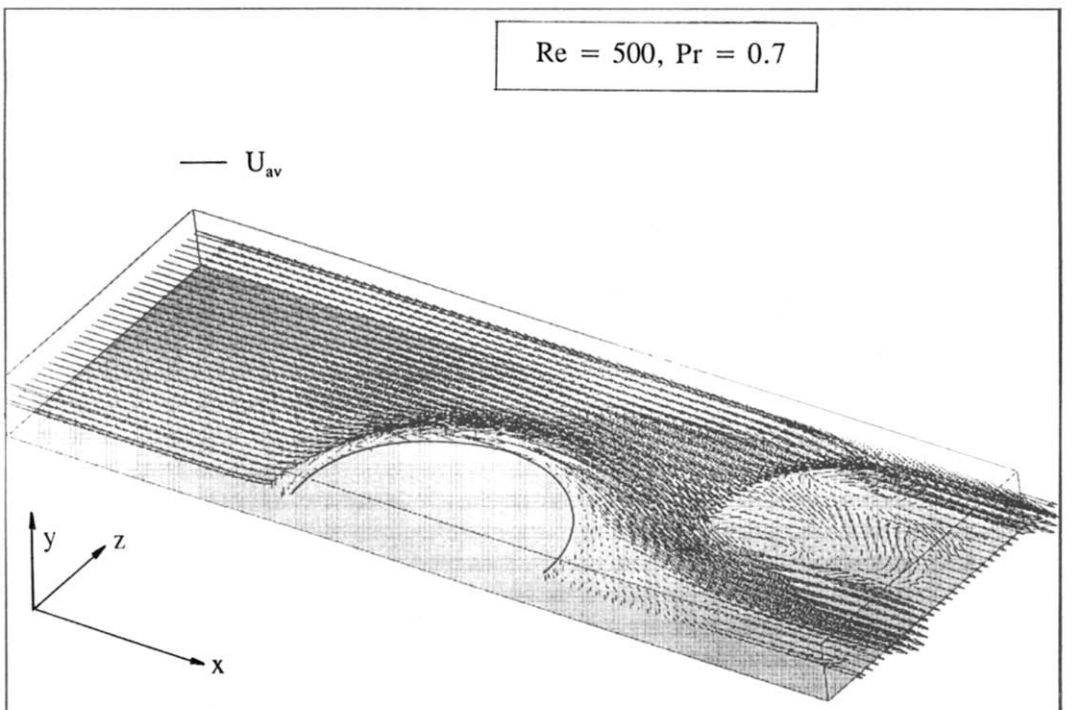

Fig. 6 Longitudinal velocity vectors at a vertical location (Y=0.416) of the channel

FIG. 6. Longitudinal velocity vectors at vertical location ($Y = 0.416$) of the channel.

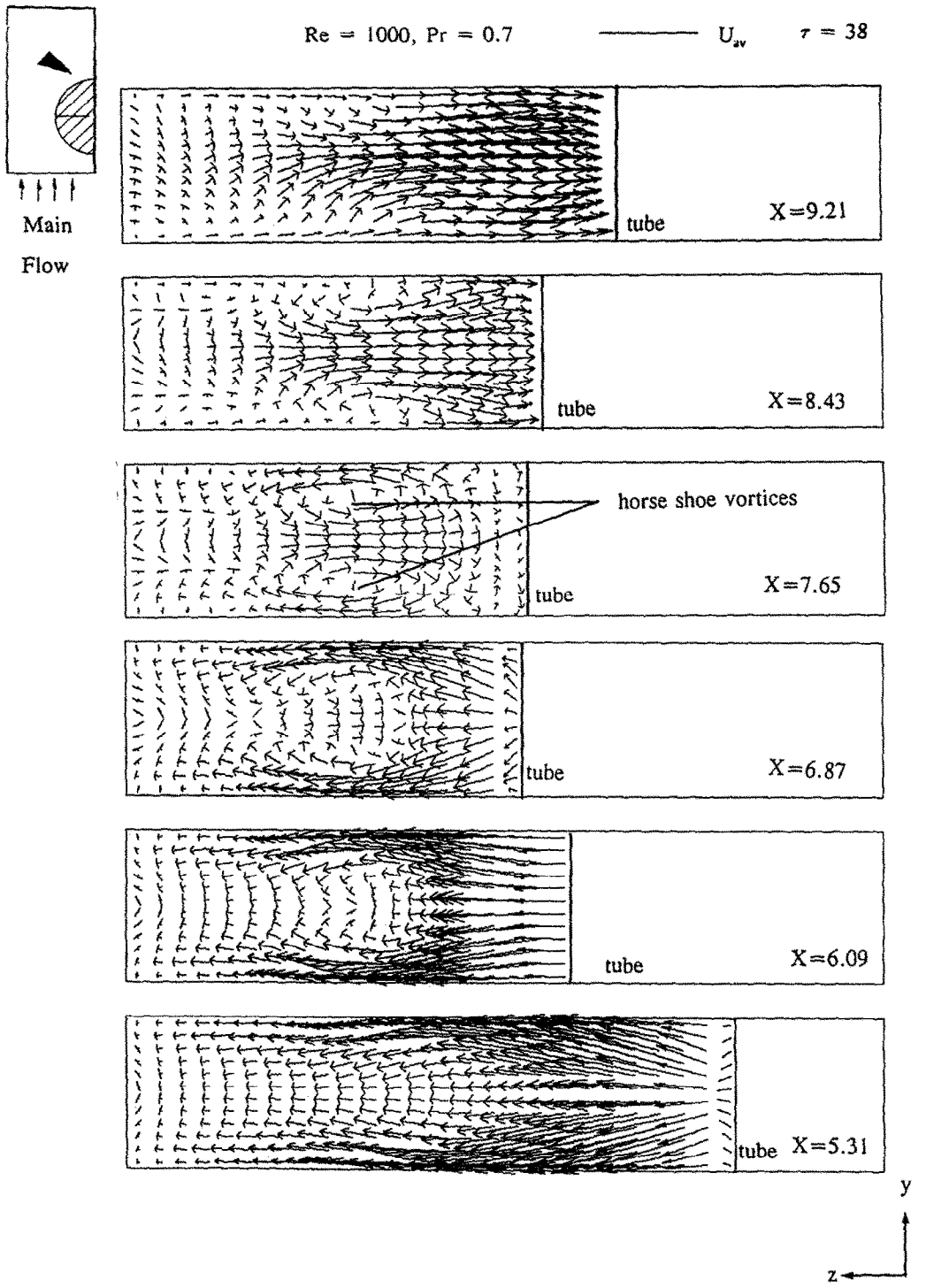

FIG. 7(a). Cross-stream velocity vectors at different axial locations from the inlet.

vortex system is formed in front of the tube which bends around the tube and forms two longitudinal vortex pairs on two sides of the symmetry plane. The development of crossflow, due to the winglet is observed in Fig. 7(b). The maximum crossflow velocity roughly equals the mean axial velocity. The symmetry planes set limits to the possible divergence of the vortices and the solid walls restrict their vertical movement. It may be mentioned that for the above mentioned case (for a Reynolds number of 1000), the flow was found to be periodic. The periodicity was induced due to the oscillations downstream of the wake (near the exit plane) which can be attributed to the interaction between the transverse and longitudinal vortices. However, this was a low frequency oscillation and flow in the upstream was not at all

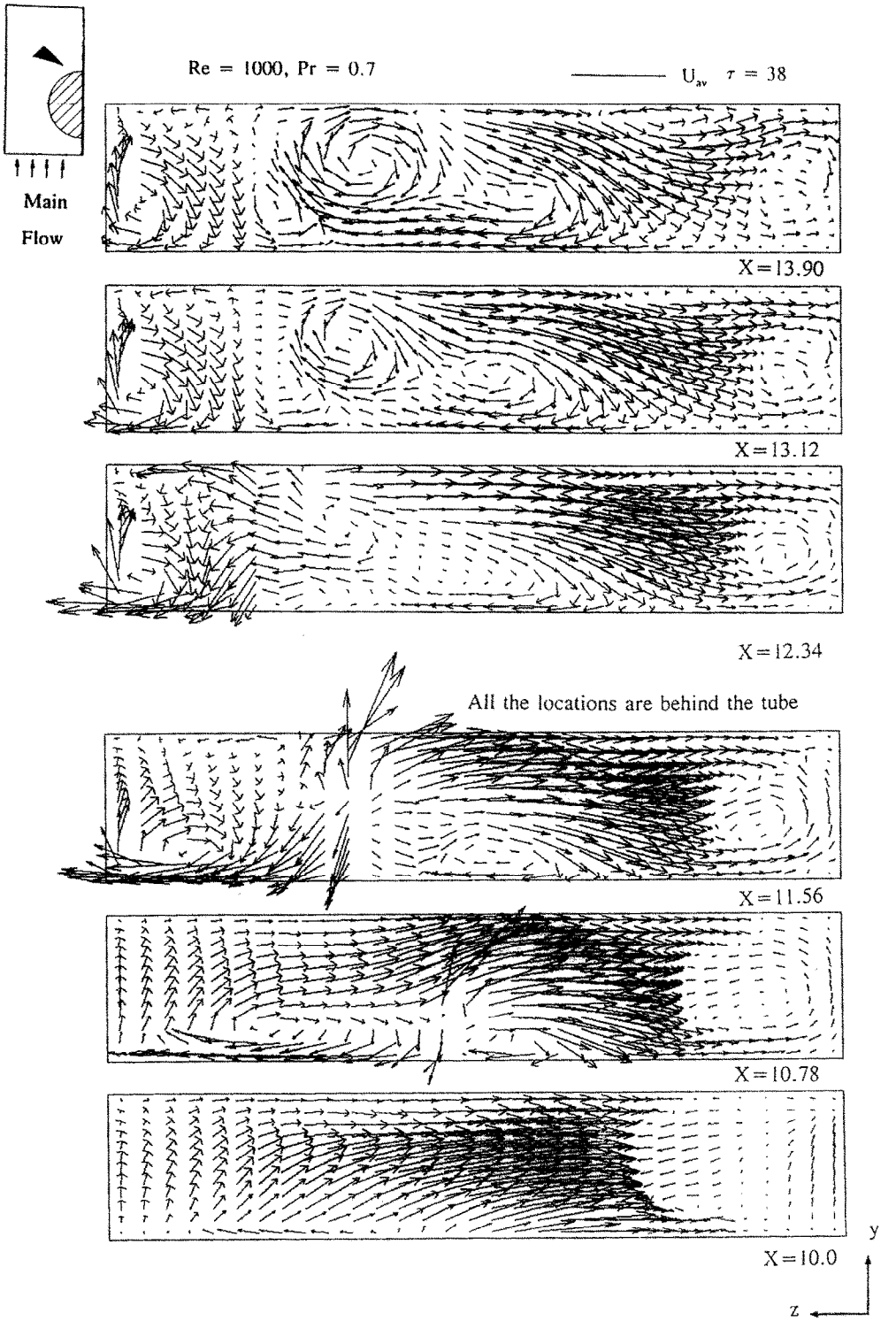

FIG. 7(b). Cross-stream velocity vectors at different axial locations from the inlet.

disturbed. The velocity-vector plots, presented here, are taken at a nondimensional time of $\tau = 38$.

Figure 8(a) shows the temperature distribution at a horizontal plane close to the bottom wall ($Y = 0.0416$). The temperature fields shows a dip at a location immediate before the forward stagnation point. This is a result of cold fluid moving downward from the symmetry plane to the bottom plate; see Fig. 8(b). It appears that there is a small zone where the fluid is trapped between the bottom plate, cylindrical tube and the horseshoe vortex. The fluid at that location rolls up and eventually culminates in a small vortex (see Goldstein and Karni [14]). However, the small vortex is heated up at the corner between the

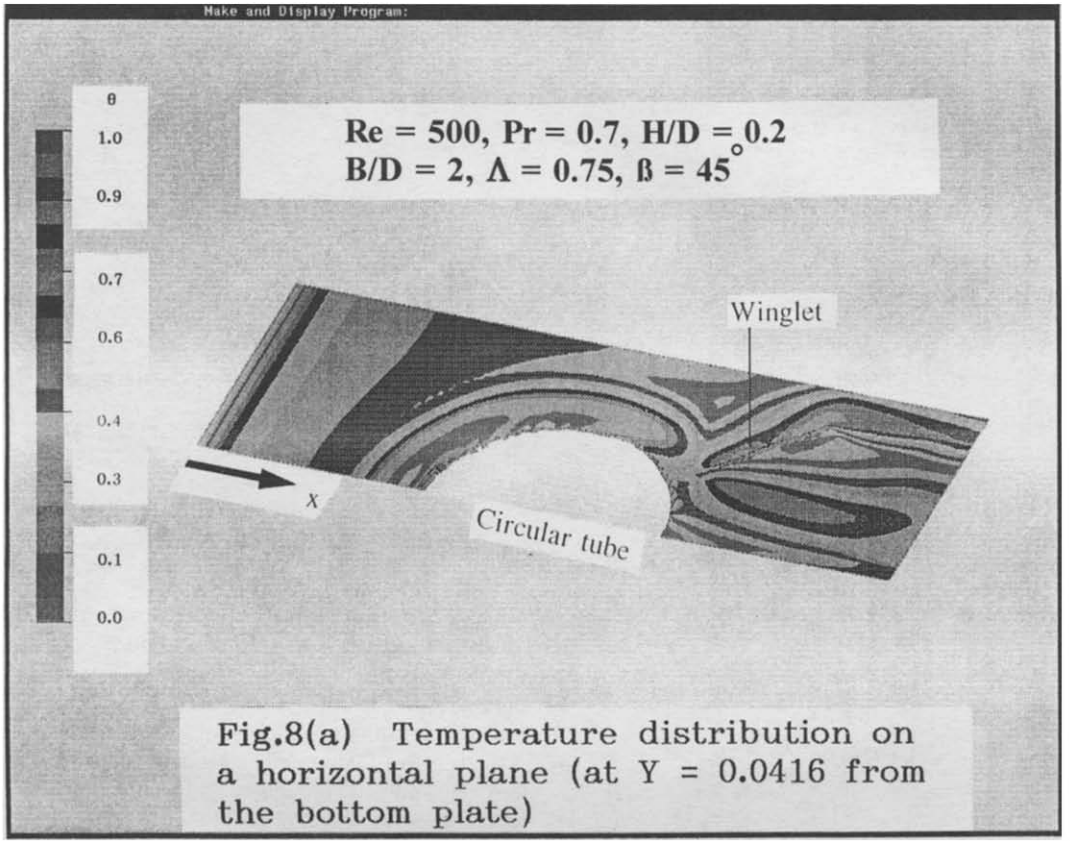

(a)

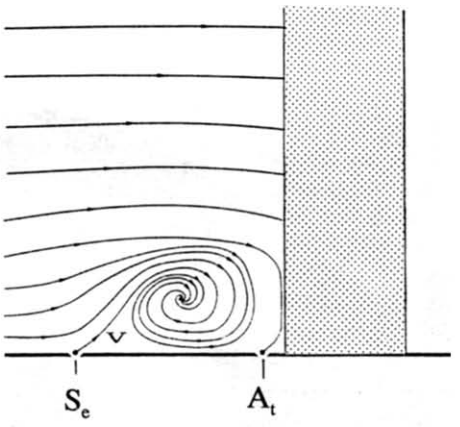

(b)

FIG. 8. (a) Temperature distribution on a horizontal lane (at $Y = 0.0416$ from the bottom plate). (b) Formation of horseshoe vortex system; S_e—separation point, A_t—attachment point, V—the vortex system (after Goldstein and Karni [14]).

tube wall and the plate and there is a rise in local temperature. This is also evident in Fig. 8(a). Behind the vortex generator, fluid temperature appears to be low at many places. This is attributed to the mixing of cold fluid from the free stream with the relatively hot fluid adjacent to the plate. From the temperature distribution, it is also clear that the cold fluid stream at the entrance is gradually heated up in the channel till it reaches the zone near the cylinder and thereafter due to the mixing with the cold stream from the upper horizontal layers, several low temperature zones are produced on the same plane. However, the temperature distribution on this plane directly affects the heat transfer from the bottom plate. Heat flux from the wall is more in the regime of low-temperature zones of the fluid.

The heat transfer performance is well understood from the combined-spanwise-average Nusselt number

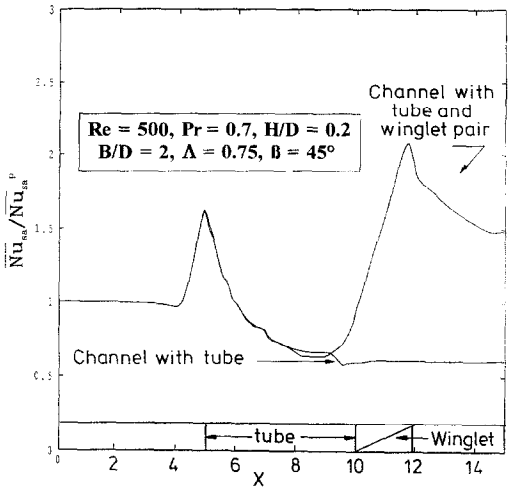

FIG. 9. Effect of the tube and the winglet on $\overline{Nu}_{sa}/\overline{Nu}^{p}_{sa}$ distribution in the channel.

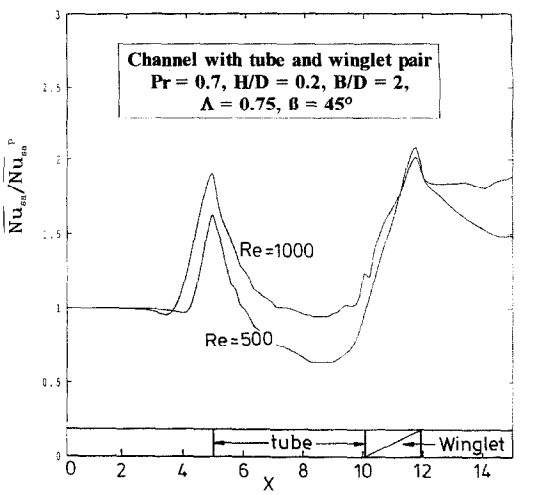

FIG. 10. Effects of Reynolds number on the distribution of $\overline{Nu}_{sa}/\overline{Nu}^{p}_{sa}$ in the channel.

distribution in the channel which is defined as

$$\overline{Nu}_{sa} = \frac{B(q_1+q_2)(H/k)}{2\left[\int_0^{B/2}(T_{w1}(x,z)-T_b(x))\,dZ + \int_0^{B/2}(T_{w2}(x,z)-T_b(x))\,dz\right]} \quad (5)$$

The effects due to the circular obstacle and the influence of protruding winglet on the wall heat transfer is presented in terms of ratio (G) of $\overline{Nu}_{sa}/\overline{Nu}^{p}_{sa}$, and $\overline{Nu}^{p}_{sa}$ signifies heat transfer performance of a plane channel. Figure 9 presents the combined spanwise average heat transfer distribution in the form of G. This includes the area with zero heat transfer on the plates covered by the tube. The variations of G along the streamwise direction of the channel for the cases with a built-in tube and with a built-in tube and a winglet are revealed in this plot. Here again, near the forward stagnation zone, the strong influence of the entrainment of cold fluid from the plane of symmetry (which wraps around the plate and creates a horseshoe vortex system) becomes obvious. This leads to a sharp increase in G ($= 1.625$) a little before the junction of the plates and the forward stagnation point of the tube (at $X = 4.84$). In the case of a built-in tube (without vortex generator), immediately downstream of the tube, relatively little heat transfer occurs; this is a recirculation region with low speed of fluid. However, in the case of a channel with built-in tube and vortex generators, the longitudinal vortices, formed near the leading edge of the winglet, take fluid from the wake region behind the tube and swirl it around, mixing the hot fluid with relatively colder stream. The heat transfer is enhanced significantly and G reaches a value as high as 2.08 at a location $X = 11.72$. Downstream of this location G decreases gradually with x but attains a reasonably high value (1.487) at the exit of the channel. As such, at the location $X = 11.72$ in the channel, the enhancement in heat transfer is more than 240%. The effect of Reynolds number on heat transfer performances is clearly evident from Fig. 10. A higher Reynolds number signifies a higher mass flow rate and as a consequence a higher heat removal rate is observed. The flow field for $Re = 1000$ is found to be periodic, hence the heat transfer results are time-averaged values. However, at the exit of the channel ($X = 15$), G for $Re = 1000$ is 27% larger than that for $Re = 500$.

The model validation was performed through a comparison with experimental results of Valencia [8]. The combined-spanwise average Nusselt number distribution along the streamwise direction of the channel was compared (Fig. 11). The flow is developing both hydrodynamically and thermally. Reynolds number and Prandtl number for this case are 646

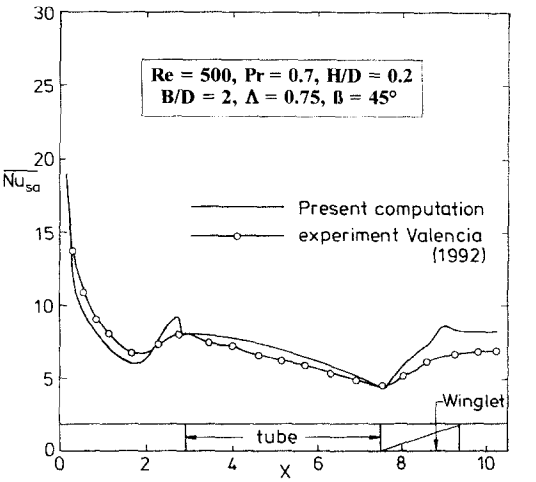

FIG. 11. Comparison of computed results with experimental results.

and 0.7, respectively. However, the computed results compare favourably with the experimental results. In some locations discrepancy is relatively high. Possibly the strength of the longitudinal vortices in computation is relatively higher than that of the experiment. Due to very small thickness (8.4×10^{-4} m) of the fin (in experiment), the axial heat conduction was not good and it was not possible to maintain perfect isothermal condition on the plate surface. Details of experimental techniques deployed in the determination of local heat transfer coefficient are available in Fiebig *et al.* [1]. Measurements were done by using unsteady liquid crystal thermography. Average values were obtained subsequently from the measured values. The RSS uncertainty described by Moffat [15] was below 4.3% for local heat transfer coefficients.

REFERENCES

1. M. Fiebig, P. Kallweit, N. K. Mitra and S. Tiggelbeck, Heat transfer enhancement and drag by longitudinal vortex generators in a channel flow, *Exp. Thermal Fluid Sci.* **4,** 103–114 (1991).
2. S. Tiggelbeck, N. K. Mitra and M. Fiebig, Flow structure and heat transfer in a channel with multiple longitudinal vortex-generators, *Exp. Thermal Fluid Sci.* **5,** 425–436 (1992).
3. M. Fiebig, U. Brockmeier, N. K. Mitra and T. Güntermann, Structure of velocity and temperature fields in laminar channel flows with longitudinal vortex generators, *Numer. Heat Transfer, Part A* **15,** 281–302 (1989).
4. U. Brockmeier, M. Fiebig, T. Güntermann and N. K. Mitra, Heat transfer enhancement in fin-plate heat exchangers by wing-type vortex generators, *Chem. Engng Technol.* **12,** 288–294 (1989).
5. G. Biswas, N. K. Mitra and M. Fiebig, Computations of laminar mixed convection flow in a channel with wing-type built-in obstacles, *J. Thermophys. Heat Transfer (AIAA)* **3,** 447–453 (1989).
6. G. Biswas and H. Chattopadhyay, Heat transfer in a channel with built-in wing-type vortex generators, *Int. J. Heat Mass Transfer* **35,** 803–814 (1992).
7. Y. Dong, Experimentelle Untersuchung de Wechselwirkung von Längswirbelerzeugern und Kreiszylindern in Kanalströmungen in Bezug auf Wärmeübergang und Strömungsverlust, Doctoral Thesis, Ruhr-Universität Bochum, Germany (1992).
8. A. Valencia, Wärmeübergang und Druckverlust in Lamellen-Rohr-Wärmeübertragern mit Längswirbelerzeugern, Doctoral Thesis, Ruhr-Universität Bochum, Germany (1992).
9. M. Sanchez, N. K. Mitra and M. Fiebig, Numerical investigations of three-dimensional laminar flows in a channel with built-in circular cylinder wing-type vortex generators, *Proc. Eighth GAMM-Conference on Numerical Methods in Fluid Mechanics (Vieweg)*, pp. 484–492 (1989).
10. F. H. Farlow and J. E. Welch, Numerical calculation of time-dependent viscous incompressible flow of fluid with free surfaces, *Phys. Fluids* **8,** 2182–2188 (1965).
11. C. W. Hirt and J. L. Cook, Calculating three-dimensional flows around structures and over rough terrain. *J. Comput. Phys.* **10,** 324–340 (1972).
12. B. E. Launder and T. H. Massey, The numerical prediction of viscous flows and heat transfer in tube-band, *J. Heat Transfer* **100,** 565–571 (1978).
13. G. D. Raithby and K. E. Torrance, Upstream-weighted differencing schemes and their applications to elliptic problems involving fluid flow, *Comput. Fluids* **2,** 191–206 (1974).
14. R. J. Goldstein and J. Karni, The effect of a wall boundary layer on a local mass transfer from a cylinder in crossflow, *J. Heat Transfer* **106,** 260–267 (1984).
15. R. J. Moffat, Describing the uncertainties in experimental results, *Exp. Thermal Fluid Science* **1,** 3–17 (1987).